

Nanoscale

Accepted Manuscript



This is an *Accepted Manuscript*, which has been through the Royal Society of Chemistry peer review process and has been accepted for publication.

Accepted Manuscripts are published online shortly after acceptance, before technical editing, formatting and proof reading. Using this free service, authors can make their results available to the community, in citable form, before we publish the edited article. We will replace this *Accepted Manuscript* with the edited and formatted *Advance Article* as soon as it is available.

You can find more information about *Accepted Manuscripts* in the [Information for Authors](#).

Please note that technical editing may introduce minor changes to the text and/or graphics, which may alter content. The journal's standard [Terms & Conditions](#) and the [Ethical guidelines](#) still apply. In no event shall the Royal Society of Chemistry be held responsible for any errors or omissions in this *Accepted Manuscript* or any consequences arising from the use of any information it contains.

Invited paper # NR-ART-12-2013-006646

Rev. 2/12/14; 12/15/13

Nanomanipulation, nanotribology and nanomechanics of Au nanorods in dry and liquid environments using an AFM and depth sensing nanoindenter

Dave Maharaj and Bharat Bhushan[†]

Nanoprobe Laboratory for Bio- & Nanotechnology and Biomimetics (NLBB)

The Ohio State University, 201 W.19th Avenue

Columbus, Ohio 43210-1142, USA

Abstract:

Nano-objects in dry and liquid conditions have shown reductions in friction and wear on the macroscale. In this research, for the first time, Au nanorods were studied on the nanoscale under dry conditions and submerged in water for their effect on friction and wear reduction. The data were compared with spherical Au nanoparticles. Atomic force microscopy (AFM) experiments on the nanoscale were performed in single-nano-object contact with an AFM tip, where nano-objects were laterally manipulated and multiple-nano-object contact with a tip attached to a glass sphere sliding over several nano-objects. Nanoscale and macroscale wear tests with an AFM and ball-on-flat tribometer were performed to relate friction and wear reduction on both scales. Results indicate that Au nano-objects contribute to friction and wear reduction due to the reduced contact area and possible rolling and sliding on the nanoscale. Compression tests (global deformation) using a nanoindenter with a flat punch was used to investigate the mechanical behavior under load and its relation to friction and wear reduction. Repeat compression tests of nano-objects were performed which showed a strain hardening effect and increased pop-ins during subsequent loads.

Keywords: Au, Nano-objects, Nanomanipulation, Friction, Wear, Compression

Corresponding author: [†] Bhushan.2@osu.edu

1. Introduction

Nano-objects have been investigated for applications that require controlled manipulation and targeting in biomedicine and the oil industry, and tribology on the macro -to nanoscale. They undergo deformation during contact with each other or between the surfaces in which they are introduced in the various applications. Knowledge of interfacial friction and wear and their mechanical properties and the deformation mechanisms involved is important for determining their suitability for various applications.

In targeted drug delivery applications, Au, Fe₂O₃, polymer and SiO₂ nano-objects have been studied.¹⁻³ In applications requiring chemical sensors, oxidized carbon black coated with oil detecting agents and composites of collagen and iron oxide nanoparticles have been used.⁴⁻⁷ In manipulation studies with an AFM under dry conditions, the contact area and relative humidity dependence of friction force have been demonstrated by several.⁸⁻¹⁴ Studies carried out in liquid environments have shown reductions in friction force.¹²⁻¹⁴

Nanoparticles including Au, carbon nanohorns (CNH), Fe₂O₃, Sb, MoS₂ and WS₂; nanorods including ZnS, ZnO and AgVO₃; and nanotubes including MoS₂, WS₂, and carbon nanotubes (CNT) have been studied in tribological applications on the macro- to nanoscale. Studies have been carried out in dry conditions on the macroscale,¹²⁻¹⁶ microscale using a surface force apparatus (SFA),^{17,18} the nanoscale using an AFM,^{9,11-14,19-22} and nanoscale using a nanomanipulator with an AFM probe inside a transmission electron microscope (TEM).^{23,24} In liquid conditions studies have also been carried out on the macroscale,^{12-15,25-29} microscale, using an SFA,^{30,31} and nanoscale using an AFM.^{12-14,32}

As discussed by Maharaj and Bhushan,¹²⁻¹⁴ increasing the lifetime and efficiency of individual components of systems in tribological applications is crucial to the commercialization of micro/nanoelectromechanical systems (MEMS/NEMS). With MEMS/NEMS devices, the initial start-up forces and torques needed become high due to adhesive and friction forces, which can hinder device operation and reliability.^{33,34} The choice of a suitable nano-object lubricant on these scales becomes crucial.

In addition to reducing friction and wear, nano-object lubricants should be able to withstand high contact pressures experienced during operation between surfaces. Nano-objects made of materials including Au, Cu, Nb and Ni have displayed enhanced mechanical properties in several studies using a depth sensing nanoindenter.³⁵⁻⁴⁰ In these nanoindentation (local

deformation) and compression (global deformation) studies it was found that hardness or yield strength increased as diameter decreased. The scale dependence was explained in terms of the dislocation starvation model or Hall-Petch effect for single crystalline and polycrystalline nano-objects.

Au nano-objects are of interest as a lubricant. In previous experiments, use of spherical Au nanoparticles (NPs) has displayed reductions in friction and wear in dry and liquid conditions.¹²⁻¹⁴ In addition to their lubricating ability, their chemical inertness, low to no toxic effects and higher hardness compared to bulk makes them attractive as a lubricant.⁴⁰

Of interest are Au nanorods (NRs). Various studies have made use of Au NRs for applications including monitoring of carbon nanotube alignment in various films,⁴¹ aspect ratio and cellular uptake for drug delivery⁴² and molecular imaging and photothermal cancer therapy.⁴³ No studies have been done in tribological applications of Au NRs on the macro-to nanoscale.

It is believed that the small contact area of the NR and mobility due to its cylindrical shape, which allows it to slide and possibly roll, is expected to result in reduced friction and wear similar to studies of MoS₂ and WS₂ nanotubes.^{13,14} Mechanisms for these reductions are depicted in **Figure 1**. **Fig. 1a-c** shows examples of rolling, sliding and dragging of nano-objects with Au NRs as an example. In the case of NRs rolling is dependent on their orientation which may affect the degree to which rolling contributes to friction and wear reduction as compared to spherical NPs. It is of interest to determine if Au NRs can still provide effective friction and wear reduction despite a lower probability of rolling compared to spherical Au NPs.

Tribological studies performed on the macro- to nanoscale by various groups showed reductions in friction and wear when nano-objects were submerged in water, dodecane and glycerol.^{12-14, 29,31} Adding Au NRs to liquids is also expected to further reduce friction and wear.

To characterize friction forces and understand the mechanism of friction and wear reduction of nano-objects, studies have been carried in both single- and multiple-nano-object contact using an AFM. In single-nano-object contact studies, nano-objects are pushed laterally using an AFM tip and provide understanding of the nature of the friction mechanism. Multiple-nano-object contact studies simulate the ensuing contacts experienced when nano-objects are introduced for the purpose of friction and wear reduction. Further studies are needed with low viscosity liquids and nano-objects made of the same materials with different shapes.

In determining the suitability of nano-objects for various applications in controlled manipulation and targeting and tribology from the macro-to-nanoscale, it is also important to study its nanomechanical behavior when subjected to an applied load. Compression studies, using a depth sensing nanoindenter, simulate the type of loading nano-objects experience in tribological applications on the macro-to nanoscale. Further studies are needed to determine how deformation mechanisms of nano-objects aid in reducing friction and wear.

Au NRs were chosen for the experiments presented in this paper. The effects of Au NRs on friction and wear in dry and submerged liquid conditions were studied using an AFM for the first time. To determine the effects of shape, spherical Au NPs were also used as a control for comparison. Macroscale ball-on-flat tests were performed to link the macroscale friction and wear to that observed on the nanoscale. Compression (global deformation) tests using various normal loads were applied through a nanoindenter using a flat punch to understand deformation behavior and its relation to friction and wear. Repeat compression tests of nano-objects were performed to study nanoscale strain hardening.

2. Experimental

2.1 Materials and Sample preparation

Si (100) silicon wafers with a native oxide layer (University Wafers, Boston, MA) were ultrasonically cleaned in DI water, followed by isopropyl alcohol (IPA) and finally acetone for 15 min each.

Spherical Au NPs and NRs (Nanopartz, Inc., Loveland, CO) were used in these experiments with the nanoparticles used as a control. The nominal diameters for the Au nano-objects as reported by the manufacturer were 50 nm (Au 50) with a NR length of about 200 nm. **Figure 2** shows transmission electron microscopy (TEM) images of the Au nano-objects.⁴⁴

For experiments involving nano-object coated surfaces in dry conditions, several droplets of Au nano-objects suspended in DI water were deposited onto clean Si (100) substrates using a syringe. A 25% concentration of an initial 0.05 mg/ml solution was used for all sliding, wear and compression experiments unless otherwise stated. The substrate was then placed on a hot plate and heated to a temperature of about 70-80 °C and left until the liquids evaporated.

For experiments on nanoparticles submerged in water, a fluid cell consisting of a standard multimode cantilever holder (Bruker, Santa Barbara, CA), with a glass plate glued just above the cantilever, was used.¹²

2.2 Single-nano-object contact - lateral manipulation of nano-objects over a silicon substrate in dry and submerged in liquid environments

In single-nano-object contact, as shown in **Fig. 3a** as an example, a sharp tip with a nominal radius of 15 nm was used to push the nano-objects laterally. This allowed for determination of the friction force between the different nano-objects and substrate and also allows for the exploration of the friction mechanism. In addition, single nano-object contact allows for the exploration of the contact area dependence of friction without an external load. This is discussed in detail by Maharaj and Bhushan.¹²

2.2.1 Nanoscale friction

Friction force data for nanoscale experiments were obtained by using a commercial AFM (Multimode, Bruker, Santa Barbara, CA). The friction signals obtained were converted to forces by using an established calibration method.^{34,45} Normal loads are determined by multiplying the cantilever vertical deflection by the cantilever stiffness.³⁴ The vertical deflection in turn was obtained by operating the cantilever in force calibration mode, in which the deflection sensitivity obtained from the force curve was multiplied by the change in setpoint voltage.

A sharp silicon nitride tip (Orc8 series, Bruker, Camarillo, CA) with $k = 0.38$ N/m and a nominal radius of 15 nm was used for manipulation of single NPs and NRs in dry conditions. A 10% concentration of NPs and NRs was used to ensure that isolated unagglomerated nano-objects could be found and would not be hindered by other nano-objects during a manipulation attempt. For submerged in water conditions, a silicon nitride tip of lower force constant was used (Orc8 series, Bruker, Camarillo, CA) with $k = 0.05$ N/m and a nominal radius of 15 nm. The average friction force value presented is the result of five manipulations.

2.3 Multiple-nano-object contact - sliding of a glass sphere over several nano-objects in dry and submerged in liquid conditions

Multiple-nano-object contact studies simulate the ensuing contacts experienced when nano-objects are introduced for the purpose of friction and wear reduction. For multiple-nano-object contact as shown in **Fig. 3b** as an example, a glass sphere attached to an AFM tip was

used to slide over several nano-objects. From this type of experiment both coefficient of friction and wear data on nano-object coated surfaces were obtained and is discussed in detail by Maharaj and Bhushan.¹²

2.3.1 Nanoscale friction

In multiple-nano-object contact, to determine the coefficient of friction, a soda lime glass sphere (Duke Scientific Corporation, Palo Alto, CA) of nominal radius 50 μm attached to a silicon probe (FORT series, Applied NanoStructures, Inc., Santa Clara, CA) with a spring constant (k) = 3 N/m was used. Friction and normal force data for nanoscale experiments were obtained by using a similar calibration method as in single-nano-object contact. The average speed of the glass sphere was 20 $\mu\text{m/s}$. Coefficient of friction data were obtained using the slope of the friction force and normal load plots from five random spots on the test samples. The load range consists of ten data points from 13 nN to 150 nN for both dry conditions and submerged in water conditions.

To determine the pressure acting on the NRs, a Hertzian contact analysis was performed. First, the number of NRs per unit area was found from analyzing topography images from wear tests, in sections outside of the wear area ($\sim 10/\mu\text{m}^2$). This was done using SPIP 5.1.11 (Image Metrology A/S, Horshølm, Denmark). Second, the contact area on a flat gold surface is calculated for a given load (0.0017 μm^2 at 13 nN and 0.0087 μm^2 at 150 nN) and knowing the particle density, the number of NRs for a given load under the glass sphere can be determined. Third, the contact pressure on a single NR is determined and this is divided by the number of NRs under the glass sphere to determine the overall contact pressure. Since number of particles under the tip is calculated to be as less than 1, a single particle was taken for stress calculations. The contact pressure range was from 0.2 GPa to 0.6 GPa in the load range used. The relevant material parameters for the Hertzian analysis are given in **Table 1**. These pressures later can be compared with that of macroscale in order to understand the scale effects in friction.

2.3.2 Nanoscale wear

Wear tests on the nanoscale were performed by using the glass sphere attached to a silicide coated cantilever (NANOSENSORS, Neuchatel, Switzerland) with $k = 40$ N/m to obtain a normal load of 20 μN . Using a similar contact analysis as in the previous section, the contact pressure on the NRs was found to be 3.1 GPa. The wear test was carried out for 1, 10 and 100 cycles at 10 Hz, over a 10 $\mu\text{m} \times 10 \mu\text{m}$ scan size. A larger scan size of 20 $\mu\text{m} \times 20 \mu\text{m}$ was then

taken of the area enclosing the wear scar for comparison. SEM micrographs were also taken of the wear scars and areas within the wear scars to determine the condition of the nanoparticles and nanotubes. Tests were not performed in liquid conditions, since, as the test is completed, nano-objects suspended in solution will continue to be deposited on the surface as the water evaporates and cover the wear area. Representative data for 5 -6 tests are summarized in the results section. All experiments were performed at room temperature (23 °C) and 50 -55 % relative humidity.

2.4 Macroscale friction and wear

For comparison to the nanoscale, macroscale friction tests were conducted using a ball-on-flat tribometer to determine if similar effects would be observed on both scales. A sapphire ball of 1.5 mm radius was fixed to a stationary holder attached to a cantilever beam and slid over the silicon substrate with a normal load of 200 mN.⁴⁸ Using a similar contact analysis as on the nanoscale, the contact pressure on the NRs was found to be 0.15 GPa. The stroke length was 10 mm with an average speed of 3.5 mm/s. A more detailed description is given by Maharaj and Bhushan.¹⁴ In liquid environments, 2-3 droplets of liquid, with and without nano-objects were deposited onto the silicon substrate with a syringe. The sapphire ball was then slid over the substrate. The coefficient of friction was obtained over 500 cycles. Wear was characterized by taking optical and SEM micrographs of the wear scars created during the test.

2.5 Compression

For compression experiments a spherical diamond tip of approximately 3.5 μm in radius was used as shown in **Figure 4a**. This can be considered to be a flat punch due to the large radius of the diamond tip compared to the nano-objects. **Fig. 4b** shows the topography map (top left) and corresponding 2-D profile (bottom left) of the flat punch. The pairs of arrows indicate the section on which the profile is taken. The dashed lines represent the sides of the holder on which the tip is glued. The single arrow points to a representative 200 nm x 200 nm section on the punch which is illustrated by the 3-D map (right). The root mean squared roughness (RMS) = 0.5 nm and the peak to valley (P-V) roughness = 5.9 nm. The low roughness allows for overall compression of the nanoparticles without indentation due to large asperities which may be present on the surface.

Three different maximum loads of 50, 200 and 400 μN known as low, intermediate and high were applied to the nano-objects. The relevant material parameters are given in **Table**

1. These pressures were used to probe the deformation mechanisms of the nano-objects. Repeat compression loading experiments, where several loads are applied to a single nanoparticle, were also performed. Experiments were carried out to explore strain hardening effects on the nanoscale as well as pop-in behavior. The range was 80-110 μN and loads were applied in increasing increments of 20 μN to obtain enough load-displacement curves to clearly observe strain hardening. The range was limited by the nano-objects either being pushed during imaging or stuck to the diamond tip during compression. This makes imaging and location of the nanoparticle impossible for further compression. The duration for loading and unloading was 20 s for all experiments.

To ensure repeatability, each experiment was performed five times and representative data are shown in the results section. All experiments were performed at room temperature (23 $^{\circ}\text{C}$) and 50 -55 % relative humidity.

3 Results and Discussion

In this section, results for experiments in single- and multiple-nano-object contact are given for dry conditions and submerged in water along with compression data. First, in single-nano-object contact, the friction forces are presented for Au NPs and NRs. Next, for multiple-nano-object contact, coefficient of friction data are given and explained in detail. In addition, wear data for both nanoscale and macroscale with and without addition of nano-objects are also presented. Morphological characterization of the nano-objects and wear scars are also performed. Finally, for compression with a flat punch, representative load-displacement curves are presented for low, intermediate and high loads. Morphological characterization, before and after deformation, is presented along with load-displacement curves for repeat compression.

3.1 Single-nano-object contact - lateral manipulation of nano-objects over a silicon substrate in dry and submerged in water environments

For single-nano-object contact under dry conditions, a sharp tip is used to push the nano-objects in the lateral direction.¹²⁻¹⁴ **Figure 5** shows examples of topography maps of Au NPs and NRs, highlighted by the squares, before and after manipulation within the same scan area under dry conditions. Examples of Au NPs and NRs, manipulated during imaging, submerged in water are also shown. In **Fig. 5a**, under dry conditions, this takes place on the scan line illustrated by the black arrows which also corresponds to the scan line on which the nano-object profile is

taken before manipulation. The profile of the nano-object after manipulation is taken on the scan line indicated by the white arrows. A normal load of 10 nN is used during imaging. A $2\ \mu\text{m} \times 2\ \mu\text{m}$ scan area is used and shows that the nano-objects were pushed out of the scan area. For the manipulation process a normal load of 150 nN is used to ensure the AFM tip stays on the substrate and not trace the nano-object topography. For the NPs, which are spherical in nature, the manipulation can involve rolling, sliding, and rotation about the vertical axis.²⁰ As discussed by Maharaj and Bhushan¹³⁻¹⁴ for nanotubes, in the case of the NRs within the squares, manipulation can involve rolling, sliding as well as in-plane rotation which occurs at a pivot point. This can happen when the nanorods are not pushed directly at the center of its length. Similar observations were found for manipulations of carbon nanotubes on mica and graphite.⁴⁹

Examples of lateral manipulation of Au NPs and NRs submerged in water are shown in **Fig. 5b**. A $10\ \mu\text{m} \times 10\ \mu\text{m}$ area is imaged which allows for multiple manipulations within a single topography map at a normal load of 1 nN. This load is the lowest load possible load that ensures the tip stays on the substrate and allows partial images to be obtained, since the nano-objects are weakly adhered to the surface. Partial images of the nano-objects are shown within the squares as an example, are obtained in each case. Since the nano-objects are manipulated with the same normal load used during imaging, they can no longer be found after being pushed and it is not possible to show topography and height profiles after manipulation as discussed by Maharaj and Bhushan.¹²⁻¹⁴ Initially the nano-objects are imaged as the AFM tip is able to follow their topographies. During the imaging process, as the tip repeatedly impacts the nano-objects, they become dislodged as the weak adhesive forces are overcome and the nano-objects are subsequently pushed.¹²⁻¹⁴

From the manipulation of the nano-objects, friction forces are obtained and are presented in **Figure 6** for dry and submerged in water conditions. The friction force is the average of five manipulations as mentioned in the experimental section. The friction force is the result of adhesion of the nano-objects to the substrate. The nano-objects are pushed from the side with no external load being applied to them and the friction force is dependent on the contact area. The adhesive force can include both van der Waals and meniscus forces for dry conditions as discussed by Maharaj and Bhushan;¹²⁻¹⁴ however under water conditions, meniscus forces are eliminated and much of the van der Waals forces is shielded.

The friction force data for the NPs and NRs in dry conditions is shown in **Fig. 6a**. There is an overall trend towards lower friction forces for the NPs compared to the NRs. Since the adhesive force is dependent on surface area, it is expected that the NRs will have a larger associated friction force. The results shown in **Fig. 6a-b** confirm this for both dry and submerged in water conditions.

Figure 6b presents the friction forces for the NPs and NRs submerged in water conditions. The vertical scale is magnified for data in water in order to discern the difference in friction force for the NPs and NRs. In water, the adhesive forces are due to van der Waals interactions since meniscus forces are eliminated under the submerged in water condition. The lower friction forces under the submerged in water conditions compared to the dry conditions can be attributed to the elimination of meniscus forces and nano-objects sliding on a low shear strength surface. The lower friction forces occur with the NPs due to the lower contact area independent of an applied normal load.

3.2 Multiple-nano-object contact- sliding of a glass sphere over several nano-objects in dry and submerged in water conditions

3.2.1 Nanoscale Friction

In multiple-nano-object contact, the effect of normal load acting on the Au NPs and NRs is studied along with friction force to determine the coefficient of friction. The contact pressure on the NRs was between 0.2 to 0.6 GPa. At these pressures it is expected that any capping agent which is used to prevent agglomeration of the nano-objects would be removed during friction tests. This ensures that coefficient of friction recorded results from interaction with the nano-object and the silicon substrate.

Figure 7 summarizes the coefficient of friction for dry and submerged in water conditions. Sliding in multiple-nano-object contact results in lower coefficients of friction for all cases compared to sliding on the bare silicon substrate. For sliding on NPs and NRs, the coefficient of friction reduction can be attributed to the mobility of the nano-objects in addition to the reduced contact area. As discussed by Maharaj and Bhushan,¹³⁻¹⁴ it is expected that as the glass sphere comes into contact with the nano-objects, some of them maybe deformed, since the larger nano-objects would be encountered first and experience the highest contact pressures, due to fewer nano-objects to support the normal load. The resulting friction reduction mechanism can thus be attributed to the reduced contact area, the sliding over deformed nano-objects as well as the

individual NPs and NRs dragged with the glass sphere as shown in **Fig. 1b-c**. It is also possible, as the glass sphere encounters a greater number of nano-objects the contact pressure is reduced allowing undeformed nano-objects to roll between the surfaces as shown in **Fig. 1a**. In this case, for the NPs there is a greater probability of rolling since the geometry of the NRs allows it to roll if the NR is oriented approximately perpendicular to the direction of sliding.

In dry conditions, as in single nano-object contact for the NPs, the reduced contact area of the NPs is responsible for the lower coefficient of friction along with having a higher probability of rolling. The reduced contact area also reduces load independent adhesion arising from the effects of van der Waals and meniscus forces as there is less asperity contact between the glass sphere and the silicon substrate

In submerged in water conditions the coefficients of friction were lower compared to dry conditions. Due to the low viscosity of water and the low speed of 20 $\mu\text{m/s}$ of the glass sphere, it is expected that the system operates in the boundary lubrication regime. The elimination of the meniscus forces together with sliding on a surface of low shear strength⁵⁰ due to a thin water film results in overall lower coefficients of friction compared to dry conditions for both NPs and NRs. Despite the lower probability of rolling and higher contact area, the NRs significantly lower the coefficient of friction during sliding and are comparable to the NPs when submerged in water. This is due to the fact that the water provides a surface that is easily sheared and sliding is more likely to be initiated before rolling and this together with the elimination of contact area dependent meniscus forces allows the NRs to perform almost as well as the NPs. In addition, compared to single-nano-object contact, sliding on several NPs or NRs can result in some agglomeration of nano-objects which contributes to a reduced ability to roll for both types of nano-objects.

3.2.2 Nanoscale Wear

The ability to reduce wear of the underlying surface, in addition to reducing coefficient of friction must also be considered for a prospective lubricant. **Figure 8** summarizes the wear data for sliding on Si, and Si coated with Au NPs and NRs, for 1, 10, and 100 cycles under a normal load of 20 μN in dry conditions. Tests were not performed in liquid conditions, since, as the test is completed, nano-objects suspended in solution will continue to be deposited on the surface as the water evaporates and cover the wear area. A 20 $\mu\text{m} \times 20 \mu\text{m}$ area is imaged to show wear

scars which are created over a $10\ \mu\text{m} \times 10\ \mu\text{m}$ area. Topography maps along with corresponding height profiles are also shown.

After 1 cycle the surface of the uncoated silicon appears rough during the early stages of wear as it becomes damaged.^{13,14} For the Au NP and NR coated surface, after 1 cycle the nano-objects are just beginning to be pushed out of the wear area. After 10 cycles the topography profile of the uncoated silicon surface appears smoother than after 1 cycle. This is likely due to breaking and removal of sharp asperities and eventual polishing of the surface.^{13,14} For the coated surfaces, the Au NPs and NRs agglomerate around the edges of the wear scar. For the uncoated silicon substrate after 100 cycles a small amount of material is removed with a wear depth of approximately 0.3 nm as seen in the height profile. For the coated surfaces the nano-objects are completely removed.

Figure 9 shows SEM micrographs of the wear scars in dry conditions (First row) after 100 cycles. Magnified micrographs of the areas within the squares are shown in the second row as indicated by the vertical arrows. In the magnified micrographs wear debris shows agglomerated Au NPs and NRs are pointed out by arrows within each micrograph. This debris consists of mostly crushed Au nano-objects with very little silicon. As mentioned in the previous paragraph and shown in **Fig. 8** only a small amount of silicon is removed from the bare substrate.

It is believed, since the nano-objects remain in the wear area after 1 cycle, that the damage of the silicon surface should be less than that of an initially uncoated substrate. This occurs since the nano-objects are believed to roll and slide between the glass sphere and the substrate which promotes facile shearing of the two surfaces as shown in **Fig. 1a-c**, in addition to the reduced contact area provided by the nano-objects. The NRs due to their larger surface area compared to the NPs will have a lower contact pressure acting on them and would be better able to support the applied load and provide more resistance to deformation over a longer period of time. After 100 cycles, it is therefore expected that the greatest wear occurs on the bare silicon substrate and the least wear occurs with the NRs.

3.3 Macroscale friction and wear

In macroscale friction and wear tests a sapphire ball with a radius of 1.5 mm was slid over Au NP and NR coated and uncoated silicon substrates under a normal load of 200 mN. This was carried out for 500 cycles over a stroke length of 10 mm and velocity of 3.5 mm/s. A contact

pressure of 0.15 GPa for the NRs was found as explained on the nanoscale. These conditions create a boundary lubrication regime similar to the nanoscale.

Optical micrographs of wear scars under dry and water conditions with and without the nano-objects are shown in **Fig. 10a**. In general, the widths of the wear scars shown, are larger for sliding under dry conditions compared to sliding under water conditions, as the amount of wear is greater. A greater amount of wear is seen without the nano-objects in dry and water conditions compared to cases where the NPs and NRs are added.

Figure 10b shows magnified SEM micrographs of wear scars for Au NPs and NRs in dry conditions. Agglomerations of NPs and NRs within the squares can be observed. This is in contrast to **Fig. 2a** and **Fig. 2b**, which shows TEM images of single unagglomerated nano-objects. Agglomeration occurs during the wear process as nano-objects stick together due to attractive van der Waals and meniscus forces.

Figure 11 shows the coefficient of friction data for all wear cases for 500 cycles. The coefficient of friction is higher under dry conditions, which corresponds to higher wear as seen in **Fig. 10a**. The lowest coefficient of friction coincides with the cases of least wear observed in **Fig. 10a**. Compared to the nanoscale, the coefficients of friction are higher when sliding on the NRs despite higher contact pressures on the nanoscale. As reported earlier, on nanoscale, the contact pressure range was from 0.2-0.6 GPa and for the macroscale, it was 0.15 GPa. Higher contact pressures generally lead to an increase in contact area and therefore greater friction forces. However, on the nanoscale due to the small radius of the sliding ball (50 μm), this is not significant in relation to the macroscale. On the macroscale due to the large radius of the ball (1.5 mm) there is much greater number of NRs (6420) that make contact with the ball and the silicon substrate as compared to a single NR on the nanoscale. Because of this increased contact, the friction forces are greater resulting in larger coefficients of friction.

On the macroscale, the addition of Au NPs and NRs in general results in the lower coefficients of friction for all wear cases compared to the bare silicon substrate. The nano-objects create a barrier between the two surfaces and reduce the contact area. Studies by Tevet et al.²⁴ suggested that under a higher contact pressure, using single inorganic fullerene (IF) MoS₂ and WS₂ nano-objects, sliding is more likely to take place and at lower pressures, rolling occurs. As discussed by Maharaj and Bhushan^{13,14} a similar mechanism is proposed for the macroscale wear test. It is believed that the reduction in the friction coefficient is due to sliding on the deformed

or crushed NPs and NRs, where deformation can occur when initial contact is made with larger nano-objects which are fewer in number, resulting in higher contact pressures. It is also expected that some nano-objects will be dragged along with the sapphire ball as the number of cycles increases. As more nano-objects support the load the contact pressure is reduced. This increases the chance of rolling of the undeformed nano-objects as part of the friction reduction mechanism. Similar to multiple-nano-object contact on the nanoscale, a greater probability of rolling is expected with the NPs compared to the NRs. These mechanisms are illustrated in **Fig. 1a-c** and are believed to be responsible for the lower coefficient of friction. The coefficient of friction is lower for the NPs compared to the NRs due to the lower contact area and greater probability of rolling. However, the NRs still help to reduce the friction coefficient significantly compared to sliding on the bare substrate.

Under liquid conditions the results are similar to the nanoscale, where the coefficients of friction are lower than under the dry conditions in general. This is due to the presence of a surface of low shear strength for sliding. Under submerged in water conditions the NPs provide the lower coefficient of friction. Aside from the reduced contact area, there is a greater chance of rolling with the NPs than with the NRs, similar to dry conditions.

3.4 Compression with a flat punch – Deformation of entire Au NPs and NRs

NPs and NRs have shown the ability to reduce friction and wear on both the macro- to nanoscale, as discussed in the previous sections, under an applied load. To fully understand the nanomechanical behavior, compression tests (global deformation) were carried out to simulate the type of loading the nano-objects experience under various friction and wear conditions. For this purpose, a tip, approximately 3.5 μm in radius, was used to carry out compression tests.

Figure 12 shows typical load displacement curves for compression of NPs and NRs at a maximum load of 50 μN , along with topography maps of the nanoparticles over a 5 μm \times 5 μm scan area and 2-D profiles before and after compression. In **Fig. 12b** the horizontal white arrows indicate the nano-objects of interest along with the section on which the profiles were taken. In the after compression profiles, the solid line depicts time after 1 min and the dashed line time after 4 min. The two profiles were examined to determine if there was recovery of the nano-objects as seen in previous studies.^{51,52} However, the before and after profiles, are essentially the same. In this case, due to the larger contact area, a lower pressure is being applied to the NRs compared to the NPs by the flat punch.

Figure 13 shows the topography maps of the nano-objects over a $5\ \mu\text{m} \times 5\ \mu\text{m}$ scan area and 2-D profiles before and after compression with an intermediate load of $200\ \mu\text{N}$. In the after compression profiles, the solid line depicts time after 1 min and the dashed line time after 4 min. It can be observed that with NPs and NRs there is some recovery as evidenced by the before and after profiles. Similar behavior was observed by Yamakov et al.⁵¹ using molecular dynamics (MD) simulation on nanocrystalline aluminum and Gerberich et al.⁵² during compression of Si nanoparticles using a nanoindenter. Under high stress dislocations are generated and move towards the center of the grain. Upon removal of this stress, the dislocations glide back to their source, resulting in the observed recovery or reverse plasticity. It is believed that this recovery can aid in the Au nano-objects retaining their spherical or cylindrical shapes which helps to reduce friction and wear through rolling as discussed in the section 3 for from the macro-to nanoscale. In addition, this resistance to deformation prevents the nano-objects from being easily flattened and this results in a reduced contact area also resulting in lower friction and wear as previously discussed.

Figure 14 shows examples of load displacement curves at intermediate and high loads (left) along with along with 2-D topography maps of the nano-objects over a $5\ \mu\text{m} \times 5\ \mu\text{m}$ scan area and profiles before and after compression (right). The intermediate and high loads were 200 and $400\ \mu\text{N}$. The horizontal white arrows in the topography maps indicate the nanoparticle of interest along with the section on which the profiles were taken. In the after compression profiles, the solid line depicts time after 1 min and the dashed line, time after 4 min.

The after compression topography maps and 2-D profiles (right), are for loading at high loads. The profiles shown after indentation at 1 and 4 min are essentially the same, as no recovery occurs due to the nano-objects being crushed. Topography maps and profiles were previously shown in **Fig. 13** for the intermediate loads. Similar to the low loads in **Fig. 13a**, there is greater displacement associated with NPs compared to the NRs as evidenced by the load-displacement curves due to the greater contact area. The enhanced ability NRs to resist deformation indicates its ability to be used under more severe loading conditions compared to the NPs. In these conditions the ability to maintain its shape would increase friction reduction and wear protection compared to the NPs.

Repeat compression test were also performed with increasing loads. This provides an opportunity study strain hardening on the nanoscale and investigate pop-in behavior as the loads

are increased. **Figure 15** shows load displacement curves for repeat loads for the nano-objects. Loads were applied in increasing increments of 20 μN for a range 50-110 μN . As the loads are increased the displacements are either the same or less for each subsequent load displacement curve after 50 μN . This depicts a constant hardening effect up to the loads used as seen in previous experiments with Au nanoparticles 500 nm in diameter, by Maharaj and Bhushan.⁴⁰ Higher loads were not possible as the nanoparticles would either adhere to the indenter tip or slip out, resulting in the nanoparticle not being found during subsequent imaging. As discussed by Maharaj and Bhushan⁴⁰ it is believed that the dislocations generated, which are responsible for plastic deformation, either continue to pile up or the already existing dislocations created during the previous loading phase prevents movement of new dislocations, resulting in strain hardening. More distinct pop-in events were observed especially at 90 and 110 μN . These Pop-in events are the result of slip of dislocations or generation and multiplication of dislocations in neighboring grains and are discussed in greater detail by Maharaj and Bhushan.⁴⁰ The greater amount of pop-ins would indicate that the high stress generated by the accumulated dislocations from previous compressions along with newly formed dislocations eventually causes multiple slip events to occur during loading.

The hardening effect provides an even greater resistance to deformation which is beneficial for nanotribological systems where repeat compression of the nano-objects occur during use.

4. Summary

Au nanorods 50 nm in diameter and 200 nm in length were investigated for their effect on friction and wear and compared to spherical Au nanoparticles of the same diameter in dry and submerged in water conditions. The deformation behavior of the nano-objects under compression was also investigated to understand their role in friction and wear reduction. Studies were conducted in both single- and multiple-nano-object contacts with the aid of an AFM. In macroscale studies, a ball on flat tribometer was used. Compression studies (global deformation), were performed using a flat punch. This was done under three loading regimes, described as low, intermediate and high. Strain hardening compression was also performed using repeat loads.

For single-nano-object contact, addition of the NPs and NRs result in lower friction forces in dry and submerged in water conditions due to reduced contact area and ability to roll. The smaller contact area and increased probability of rolling of NPs results in lower friction

force compared to the NRs for which rolling is orientation dependent. Lower friction forces occur in submerged water conditions compared to dry conditions due to elimination of meniscus force and sliding on a low shear strength surface.

For multiple-nano-object contact, sliding over NPs and NRs, reduced coefficients of friction compared to sliding on the bare silicon substrate due to reduced contact area and rolling and sliding among the various nano-objects in dry conditions. The lower coefficient of friction occurs with the NPs compared to the other NRs due to the mechanisms mentioned for single-nano-object contact in dry conditions. In submerged water conditions the coefficient of friction was lower compared to dry conditions due to the mechanisms mentioned for single-nano-object contact. However, the coefficients of friction are similar for both NPs and NRs which is likely due to a higher probability of sliding compared to rolling for friction reduction and elimination of contact area dependent meniscus forces. In nanoscale wear experiments in dry conditions, the addition of NPs and NRs prevents the glass sphere from coming directly into contact with the surface and reduces the wear similar to multiple nano-object contact.

In macroscale studies sliding over the various nano-objects reduced friction and wear due to the mechanisms mentioned in multiple nano-object contact on the nanoscale. The lowest coefficient of friction and wear in all cases on the macroscale occur with NPs due to the reduced contact area. The coefficients of friction were also lower in submerged liquid conditions compared to dry condition due to mechanisms mentioned on the nanoscale.

For compression studies, reverse plasticity and deformation of the nano-objects were of interest. Displacement of the NRs was lower during loading compared to the NPs for low and intermediate loads due to a larger contact area and the reduced contact pressure between the flat punch and NR. This increased resistance to deformation is expected to allow NRs to be used under more severe loading conditions than NPs. Evidence of reverse plasticity was observed during unloading for the nano-objects in compression tests at intermediate loads due to the high internal stresses generated within the nano-objects, which causes dislocations to retrace their path after unloading. It is believed that this recovery can aid in nano-objects retaining their spherical or cylindrical shapes which helps to reduce friction and wear through rolling. In addition, this resistance to deformation prevents the nano-objects from being easily flattened and resulting in a reduced contact area and lower friction and wear. Repeat compression tests showed a strain hardening effect with each subsequent load. The resulting displacement at each new load

was either the same or lower than the previous. This was due to increased resistance to deformation as a result of a greater density of dislocations restricting the creation and movement of new dislocations being formed. Several pop-in effects were observed during repeat compression tests at increasing loads due to accumulation of dislocations from previous loads and formation of new dislocations.

Manipulation studies of NPs and NRs in dry and water environments to determine friction forces have been performed and will aid in better design of applications requiring controlled manipulation and targeting of nano-objects. This study also demonstrates the ability of NRs and NPs to reduce friction and wear in dry and water environments.

Compression studies (global deformation) of NPs and NRs provide fundamental understanding of the nature of mechanical behavior and helps connect the macroscale to the nanoscale. These studies aid in understanding how nano-objects and materials behave during loading and unloading and help to understand the role of nanomechanical behavior in reducing friction and wear.

5. Acknowledgments

The financial support of this research was provided by a grant from the ACS Petroleum Research Fund, Washington D.C. (Grant # 52388-ND5)

References

- 1 R. Duncan, *Nat. Rev. Drug Discov.*, 2003, **2**, 347–360.
- 2 M. Ferrari, *Nat. Rev. Cancer*, 2005, **5**, 161-171.
- 3 N.R. Panyala, E.M. Pena-Mendez and J. Havel, *J. Appl. Biomed.*, 2009, **7**, 75–91.
- 4 J. M. Berlin, J. Yu, W. Lu, E. E. Walsh, L. Zhang, P. Zhang, W. Chen, A.T. Kan, M.S. Wong, M.B. Tomson and J. M. Tour, *Energy Environ. Sci.*, 2011, **4**, 505-509.
- 5 C. Matteo, P. Candido, R. Vera and V. Francesca, *Am. J. Appl. Sci.*, 2012, **9**, 784-793.
- 6 S. Ryoo, A. R. Rahmani, K. Y. Yoon, M. Prodanovic, C. Kotsmar, T. E. Milner and C. Huh, *J. Petrol. Sci. and Eng.*, 2012, **81**, 129-144.
- 7 P. Thanikaivelan, N. T. Narayanan, B. K. Pradhan and P. M. Ajayan, *Sci. Rep.*, 2012, **2**, doi:org/10.1038/srep00230.
- 8 C. Ritter, M. Heyde, B. Stegemann, U. D. Schwarz and K. Rademann, *Langmuir*, 2002, **18**, 7798-7803.
- 9 C. Ritter, M. Heyde, B. Stegemann, K. Rademann and U. D. Schwarz, *Phys. Rev. B*, 2005, **71**, 085405.
- 10 K. Mougín, E. Gnecco, A. Rao, M.T. Cuberes, S. Jayaraman, E.W. McFarland, H. Haidara and Meyer, E., *Langmuir*, 2008, **24**, 1577-1581.
- 11 M. Palacio and B. Bhushan, *Nanotechnology*, 2008, **19**, 315710
- 12 D. Maharaj and B. Bhushan, *Beilstein J. Nanotechnol.* 2012, **3**, 759-772.
- 13 D. Maharaj and B. Bhushan, *Tribol. Lett.*, 2013a, **49**, 323-339.
- 14 D. Maharaj and B. Bhushan, *J. Colloid Interface Sci.*, 2013b, **400**, 147-160
- 15 B. Bhushan and B.K. Gupta, *Handbook of tribology: materials, coatings, and surface treatments*, McGraw-Hill, New York, 1991.
- 16 L. Rapoport, M. Lvovsky, I. Lapsker, V. Leshinsky, Y. Volovik, Y. Feldman, A. Zak and R. Tenne, *Adv. Eng. Mater.*, 2001, **3**, 71–75.
- 17 D. P. Singh, K. Polychronopoulou, C. Rebholz and S. M. Aouadi, *Nanotechnology*, 2010, **21**, 325601.
- 18 J. Zhang, and J. Zhang, *Tribo. Lett.*, 2013, **49**, 77-83.

- 19 R. Lüthi, E. Meyer, H. Haefke, L. Howald, W. Gutmannsbauer and H.-J. Güntherodt, *Science*, 1994, **266**, 1979-1981.
- 20 M. Sitti, *IEEE/ASME Trans. Mechatronics*, 2004, **9**, 343-349.
- 21 D. Dietzel, G.S. Monninghoff, L. Jansen, H. Fuchs, C. Ritter, U.D. Scharwz and A. Schirmeisen, *J. Appl. Phys.*, 2007, **102**, 084306.
- 22 X. Hui and S. Regnier, *IEEE Trans. Nanotechnol.*, 2012, **11**, 21-33.
- 23 I. Lahouij, F. Dassenoy, L. de Knoop, J-M. Martin and B. Vacher, *Tribol. Lett.*, 2011, **42**, 133-140.
- 24 O. Tevet, P. Von-Huth, R. Popovitz-Biro, R. Rosentsveig, H. D. Wagner and R. Tenne, *Proc. Natl. Acad. Sci. U SA*, 2011, **108**, 19901-19906.
- 25 L. Cizaire, B. Vacher, T. Mogne, J.M. Le Martin, L. Rapoport, A. Margolin, and R. Tenne, *Surf. Coat. Tech.*, 2002, **160**, 282-287.
- 26 R. Greenberg, G. Halperin, I. Etsion and R. Tenne, *Tribol. Lett.*, 2004, **17**, 179-186.
- 27 L. Joly-Pottuz, F. Dassenoy, M. Belin, B. Vacher, J. M. Martin and N. Fleischer, *Tribol. Lett.*, 2005, **18**, 477-485.
- 28 L. Rapoport, O. Nepomnyashchy, I. Lapsker, A. Verdyan, Y. Soifer, R. Popovitz-Biro and R. Tenne, *Tribol. Lett.*, 2005, **19**, 143-149.
- 29 J. E. St. Dennis, K. Jin, V.T. John and N. S. Pesika, *ACS Appl. Mater. Interfaces.*, 2011, **3**, 2215-2218.
- 30 D. Gourdon, M. Yasa, A. R. Godfrey, Alig, Y. Li, C. R. Safinya and J. N. Israelachvili, *Adv. Funct. Mater.*, 2004, **14**, 238-42.
- 31 M. Akbulut, N. Belman, Y. Golan and J.N. Israelachvili, *Adv. Mater.*, 2006, **18**, 2589-2592.
- 32 R. Resch, D. Lewis, S. Meltzer, N. Montoya, B. E. Koel, A. Madhukar, A. A. Requicha, and P. Will, *Ultramicroscopy.*, 2000, **82**, 135-139.
- 33 *Springer Handbook of Nanotechnology, 3rd Edition.*, ed. B. Bhushan, Springer, Heidelberg, Germany, 2010.
- 34 *Nanotribology and Nanomechanics, I and II, 3rd Edition.*, ed. B. Bhushan, Springer, Heidelberg, Germany, 2011.
- 35 L. Thilly, F. Lecouturier, J. von Stebut, *Acta Mater.*, 2003, **51**, 5049-5065.
- 36 J.R. Greer, W.C. Oliver, W.D. Nix, *Acta Mater.*, 2005, **53**, 1821-1830.

- 37 B. Wu, A. Heidelberg, J.J. Boland, *Nature Mater.*, 2005, **4**, 525-552.
- 38 Z. W. Shan, R.K. Mishra, S.A.S. Asif, O.L. Warren, A.M. Minor, *Nature Mater.*, 2008, **7**, 115-119.
- 39 M. Dietiker, Buzzi. S, Pigozzi. G, Löffler. J. F, R. Spolenak, *Acta Mater.*, 2011, **59**, 2180-2192.
- 40 D. Maharaj and B. Bhushan, *Unpublished*, 2014.
- 41 M. A. Correa-Duarte, J. Pérez-Juste, A. Sánchez-Iglesias, M. Giersig, and L. M. Liz-Marzán, *Angew. Chem. Int. Ed.*, 2005, **44**, 4375–4378.
- 42 Y. Qiu, Y. Liu, L. Wang, L. Xu, R. Bai, Y. Ji, X. Wu, Y. Zhao, Y. Li, C. Chunying, *Biomaterials*, 2010, **31**, 7606-7619.
- 43 X. Huang, I. H. El-Sayed, W. Qian, and M. A. El-Sayed, *J. Am. Chem. Soc.*, 2006, **128**, 2115-2120.
- 44 Anonymous, <[http:// www.nanopartz.com](http://www.nanopartz.com)>, 2013.
- 45 J. Ruan and B. Bhushan, *ASME J. Tribol.*, 1994, **116**, 378–88.
- 46 *Handbook of Ceramics, Glasses and Diamonds, 1st Edition.*, ed. C.A. Harper McGraw-Hill, New York, 2001.
- 47 *Handbook of the Physiochemical Properties of the Elements*, ed. G.V. Samsonov, Plenum, New York, 1968.
- 48 B. Bhushan, *Introduction to Tribology, 2nd Edition.*, Wiley, New York, 2013.
- 49 M. R. Falvo, R. M. Taylor II, A. Helser, V. Chi, F. P. Brooks Jr, S. Washburn, and R. Superfine, *Nature*, 1999, **397**, 236-238.
- 50 B. Bhushan and S. Sundararajan, *Act. Mater.*, 1998, **46**, 3793-3804.
- 51 V. Yamakov, D. Wolf, M. Salazar, S.R. Phillpot, H. Gleiter, *Acta Mater.*, 2001, **49**, 2713-2722.
- 52 W.W. Gerberich, W.M. Mook C.R. Perrey C.B. Carter M.I. Baskes R. Mukherjee A. Gidwani, J.P. Heberlein, H. McMurry, S.L. Girshick, *J. Mech. Phys. Solids*, 2003, **51**, 979-992.

Table 1. Mechanical properties of borosilicate glass, diamond, sapphire and gold.

Mechanical Properties	Borosilicate glass ⁴⁶	Diamond ⁴⁶	Sapphire ¹⁵	Gold ⁴⁷
Young's modulus (GPa)	62	1140	390	78
Poisson's ratio	0.2	0.07	0.23	0.42

Figure captions

Fig. 1. Schematic of friction and wear reducing mechanism of nano-object coated surface by (a) rolling, (b) sliding over nano-objects, (c) dragging of nano-objects. Au 50 NRs are used as an example for mechanisms shown.

Fig. 2. (a) TEM images of (a) spherical Au nanoparticles approximately 50 nm in diameter (Anonymous, 2013), (b) Au nanorods 50 nm in diameter and 200 nm in length (Anonymous, 2013).

Fig. 3. Schematics of (a) a sharp tip pushing a nano-object in single-nano-object contact and (b) a glass sphere sliding over several nano-objects in multiple-nano-object contact.

Fig. 4. (a) Schematic showing method of deformation using a flat punch for compression (global deformation) with Au nanoparticles. (b) Topography map (top) and 2-D profile (bottom) of flat punch at the section shown by the pairs of horizontal arrows along with a typical line plot (right) of a 200 x 200 nm section indicated by the single horizontal arrow.

Fig. 5. (a) Two examples of topography maps and height profiles before and after manipulation of Au 50 NPs and NRs highlighted by the squares in the same scan area. Manipulation takes place on the scan lines shown by the black arrows which also correspond to the scan line on which the 'before manipulation' profile is obtained. The white arrows indicate the scan line on which the 'after manipulation' profile is obtained. (b) Two examples of topography maps, showing nano-objects manipulated in water for Au 50 NPs and NRs

Fig. 6. Nanoscale friction force for Au NPs and NRs on the silicon substrate during manipulation, at normal loads of (a) 150 nN in air and (b) 1 nN in water. The vertical scale is magnified for data in water (b) in order to discern the difference in friction force for the NPs and NRs.

Fig. 7. Coefficients of friction on the nanoscale for both dry and submerged in water conditions, with and without nano-objects. Coefficients of friction are lower for sliding on nano-objects in all conditions with lowest values obtained in water conditions. The load range for both dry and submerged in water conditions is 13 nN to 150 nN with a minimum of ten data points. The sliding speed was 20 $\mu\text{m/s}$.

Fig. 8. Topography maps and 2-D profiles for nanoscale wear experiments, at sections shown by the arrows, after sliding at 1, 10 and 100 cycles with a normal load of 20 μN at 10 Hz on Si and Si coated with Au 50 NPs and NRs.

Fig. 9. SEM micrographs of nanoscale wear scars for Au 50 NPs and NRs in dry conditions after 100 cycles at a normal load of 20 μN (First row). The nano-objects within the squares are magnified and the vertical arrows point to those micrographs in the second row. The magnified micrographs show agglomerated Au 50 NPs and NRs as indicated by arrows within the micrographs.

Fig. 10. (a) Optical micrographs of macroscale wear scars taken after 500 cycles at a normal load of 200 mN, for friction tests, in dry and water conditions with and without Au 50 NPs and NRs. The sliding speed was 3.5 mm/s. (b) SEM micrographs of the wear scar for agglomerated Au 50 NPs and NRs in dry conditions shown within the squares.

Fig. 11. Macroscale coefficient of friction data after 500 cycles at a normal load of 200 mN, in dry and water conditions with and without Au 50 NPs and NRs.

Fig. 12. (a) Typical load-displacement curve at a maximum load of 50 μN with Au 50 NPs and NRs and (b) topography maps and 2-D profiles at sections shown by the horizontal arrows before compression (first row) and after compression (second row). The second row shows topography maps 1 min after compression and the solid lines and dashed lines show the 2-D profiles after 1 and 4 min respectively.

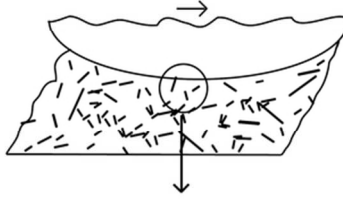
Fig. 13. Topography maps and 2-D profiles at sections shown by the horizontal arrows before compression (first row) and after compression (second row) at a maximum load of 200 μN . The second row shows topography maps 1 min after compression and the solid lines and dashed lines show the 2-D profiles after 1 and 4 min respectively. Recovery of the nanoparticles 4 min after compression demonstrates reversed plasticity.

Fig. 14. Load-displacement curves for intermediate loads 200 μN and high loads 400 μN and topography maps and 2-D profiles, at sections indicated by the horizontal arrows before compression (first row) and after compression (second row) (right). The second row shows topography maps 1 min after compression at a high load and the solid lines and dashed lines show

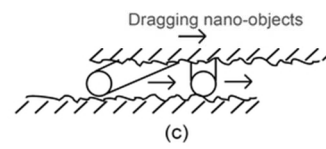
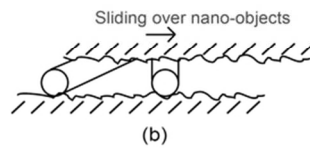
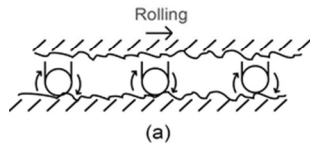
the 2-D profiles after 1 and 4 min respectively. Compression was performed on separate nano-objects for intermediate and high loads.

Fig. 15. Examples of repeat load-displacement curves for Au 50 NPs and NRs with the corresponding maximum loads for each compression event. Vertical arrows point to pop-in events. Increments were done at 20 μN for a range of 50-110 μN . Evidence of strain hardening can be seen where successive load results in the displacement being the same or less after unloading.

Friction and wear reducing mechanisms during sliding on a nano-object coated surface



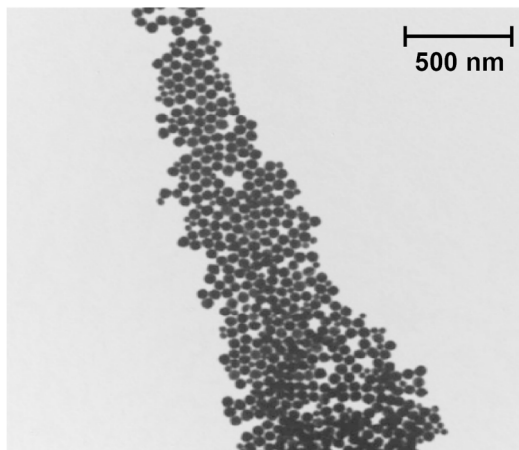
Mechanisms for spherical and tubular nano-objects with Au nanorods used as an example



74x37mm (300 x 300 DPI)

Au nanoparticles

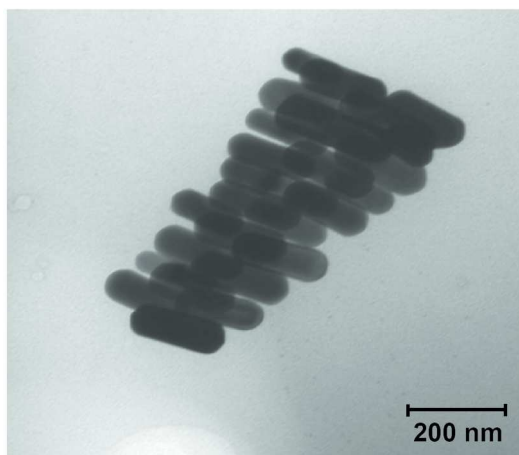
Au 50



(a)

Au nanorods

Au 50

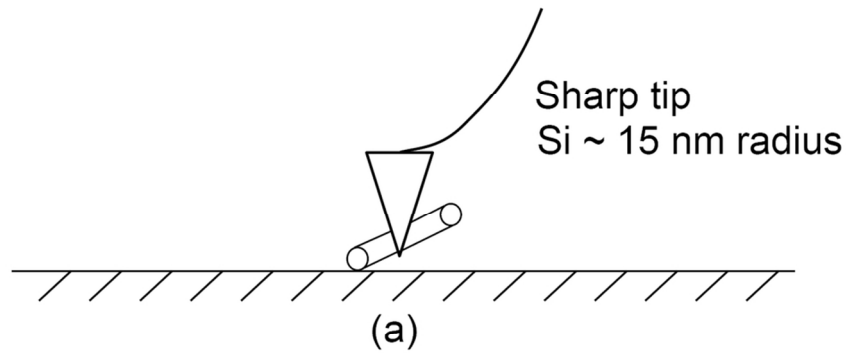


(b)

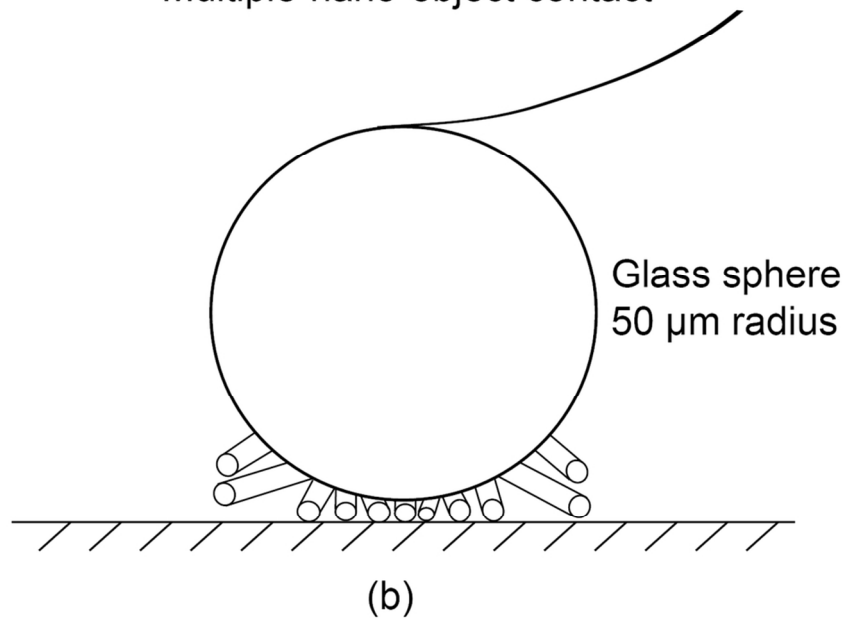
117x269mm (300 x 300 DPI)

Illustration of contact with Au nanorods

Single-nano-object contact



Multiple-nano-object contact

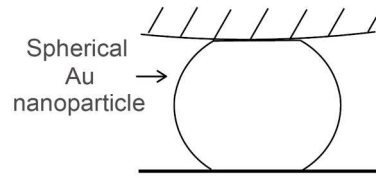


86x118mm (300 x 300 DPI)

Method of deformation

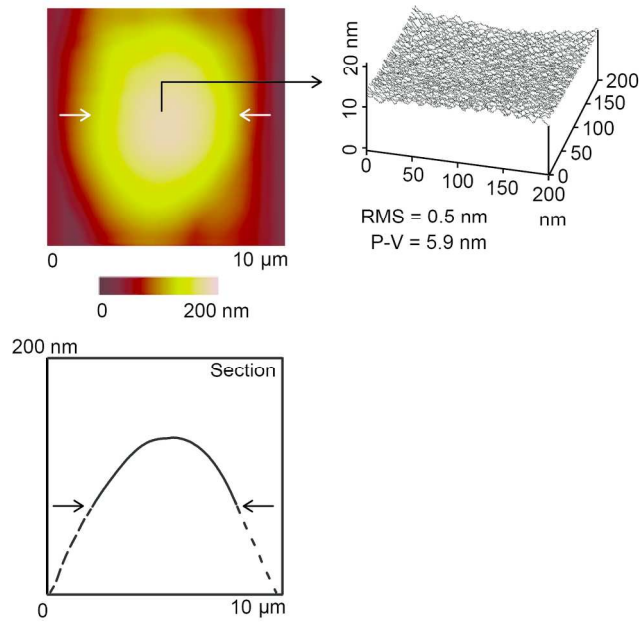
Flat punch

Compression
(global deformation)



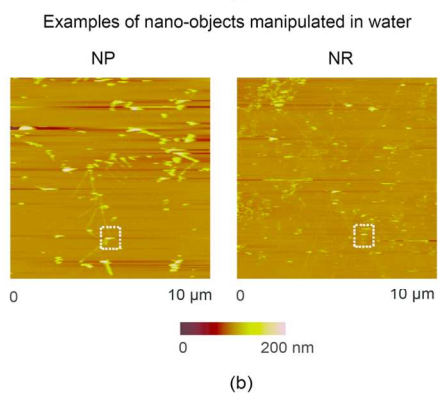
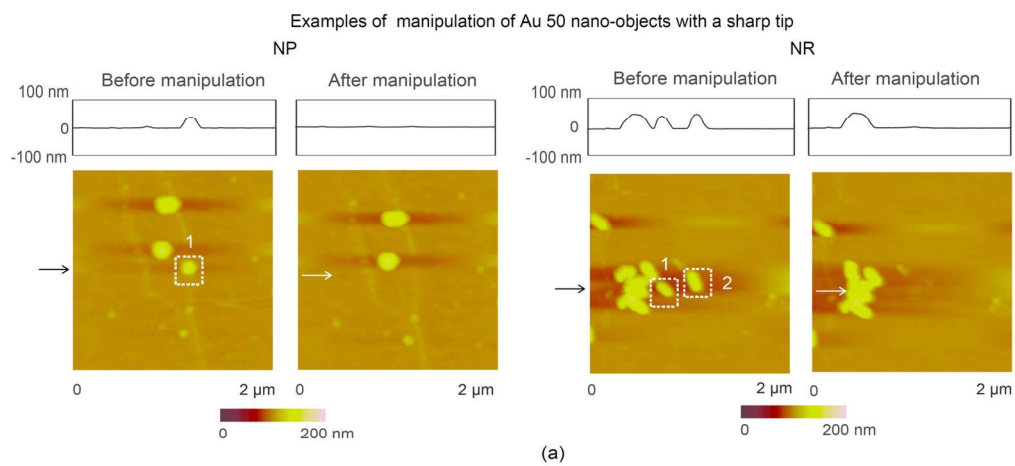
(a)

Topography and profile of flat punch

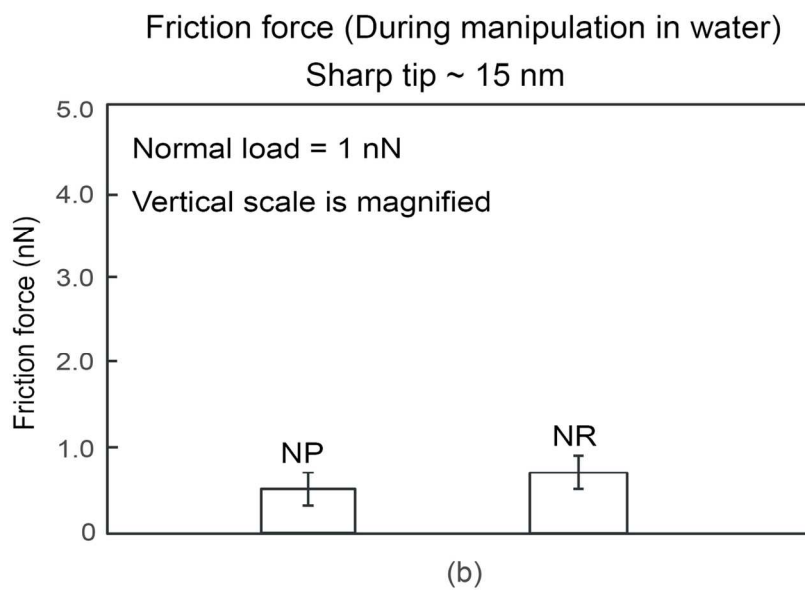
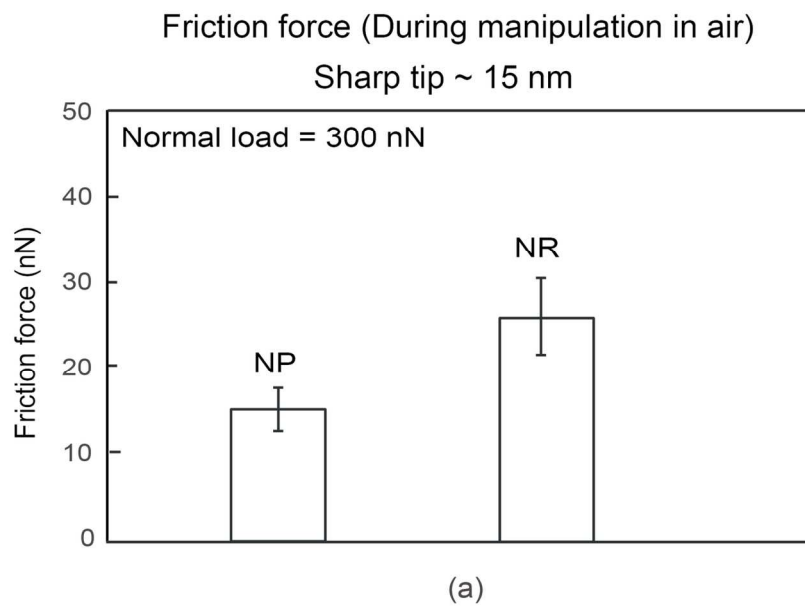


(b)

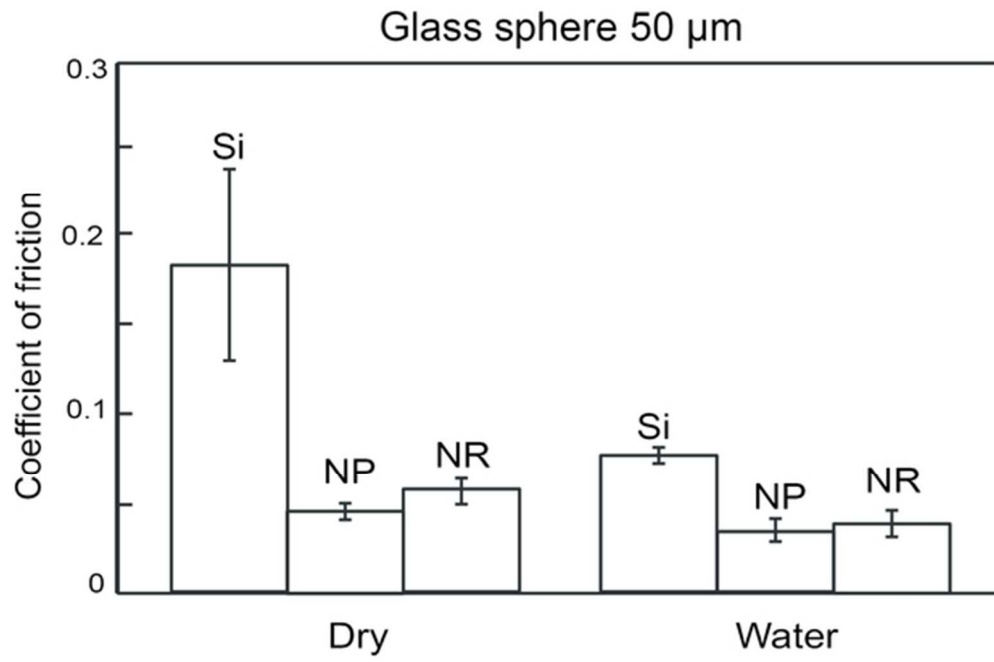
128x244mm (300 x 300 DPI)



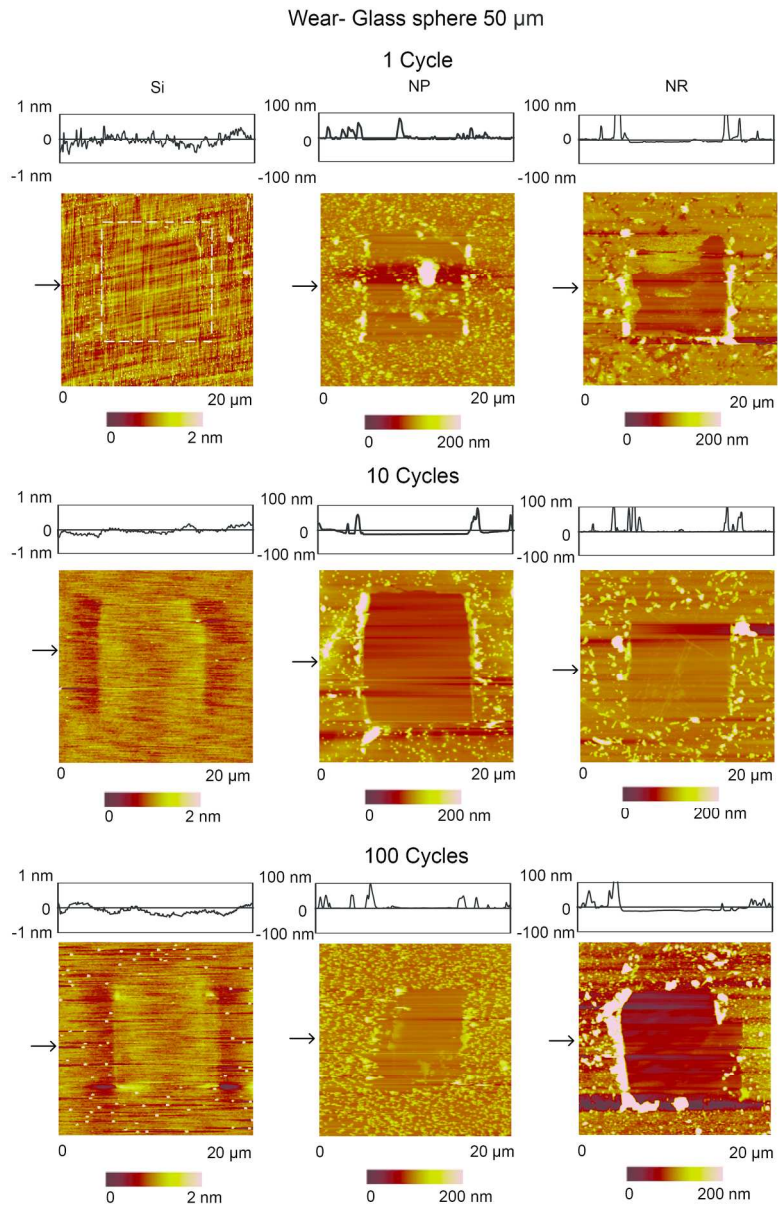
136x115mm (300 x 300 DPI)



119x170mm (300 x 300 DPI)

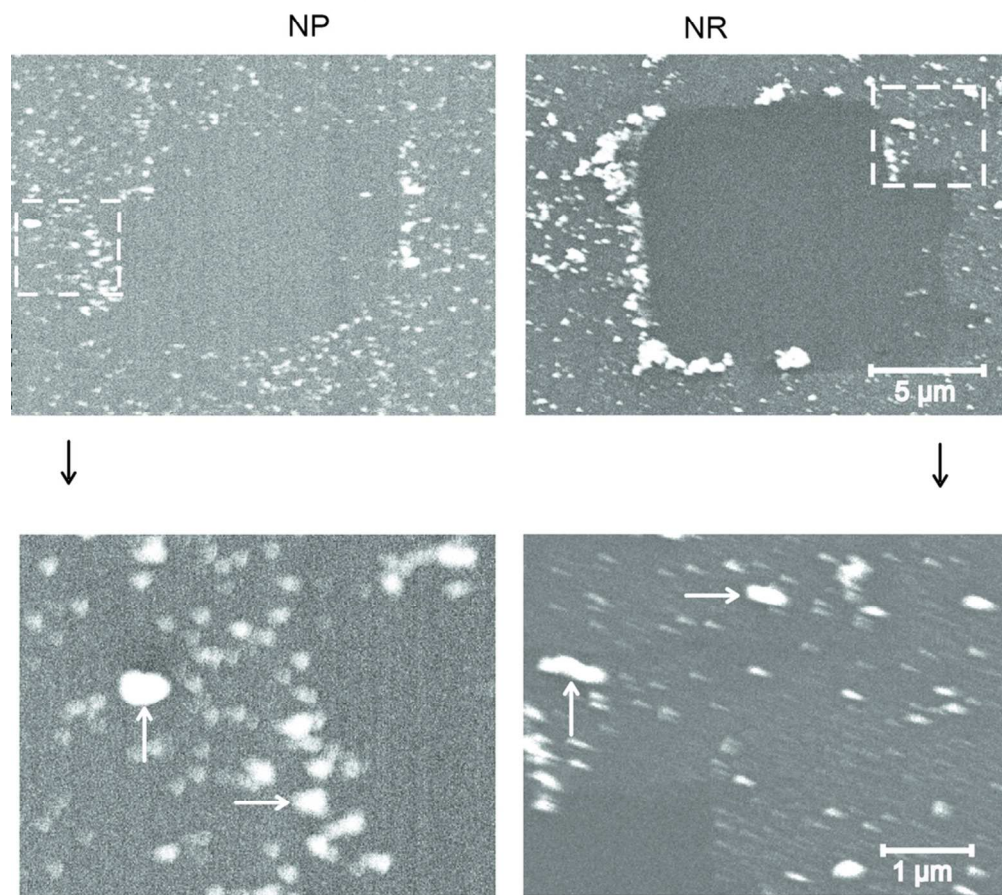


52x34mm (300 x 300 DPI)



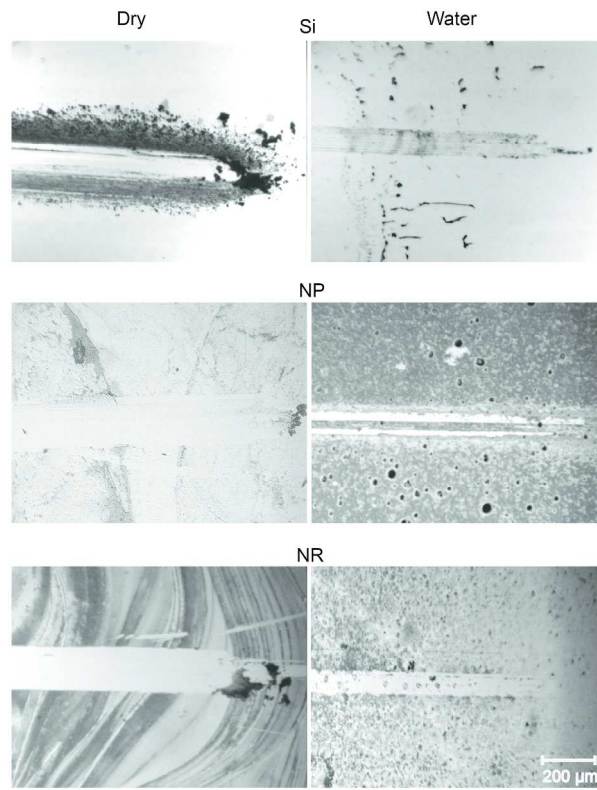
159x238mm (300 x 300 DPI)

SEM micrographs of nanoscale wear scars
in dry conditions after 100 cycles



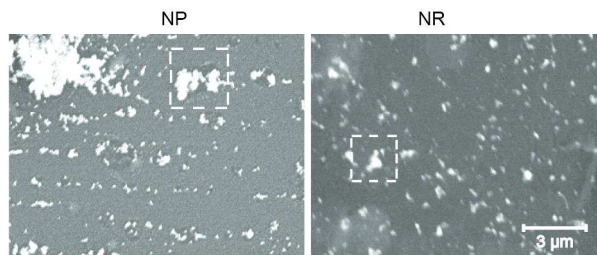
88x85mm (300 x 300 DPI)

Optical micrographs of macroscale wear scars



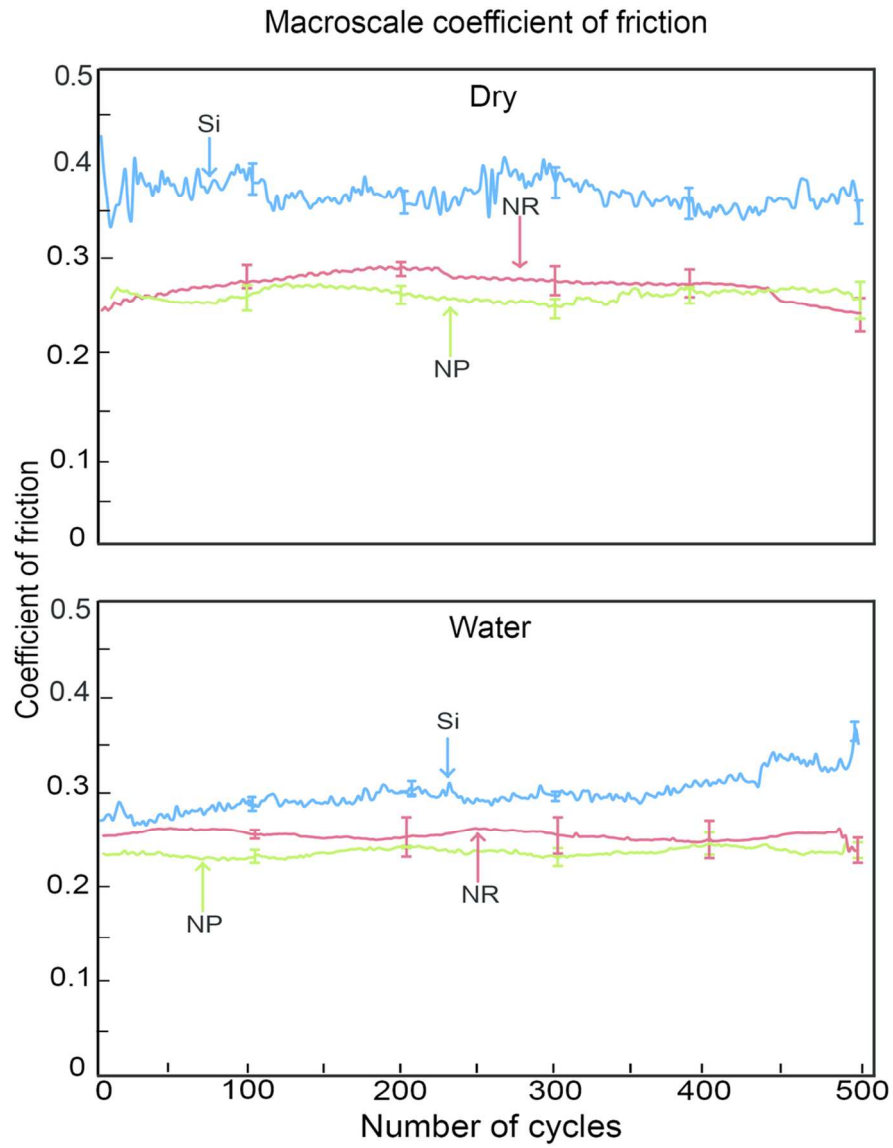
(a)

SEM micrographs of macroscale wear scars in dry conditions

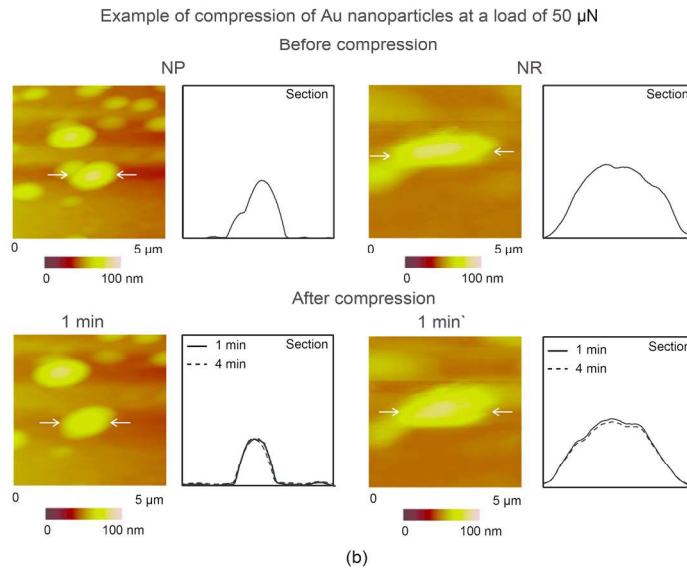
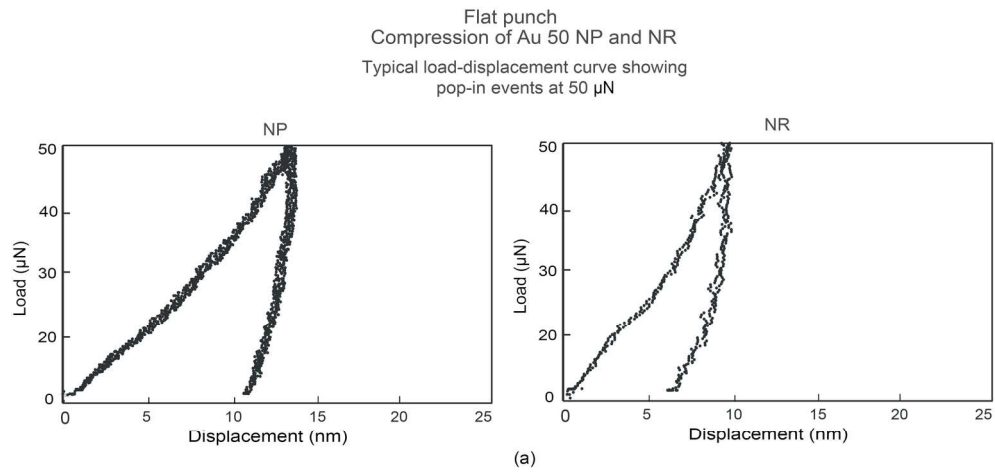


(b)

178x346mm (300 x 300 DPI)



104x121mm (300 x 300 DPI)

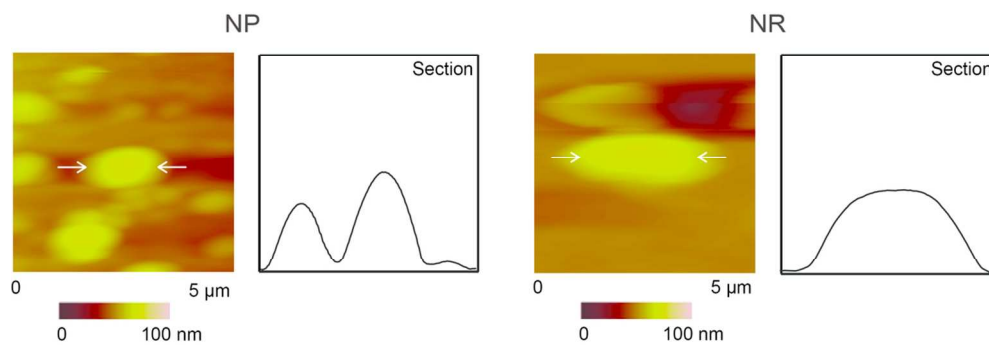


175x185mm (300 x 300 DPI)

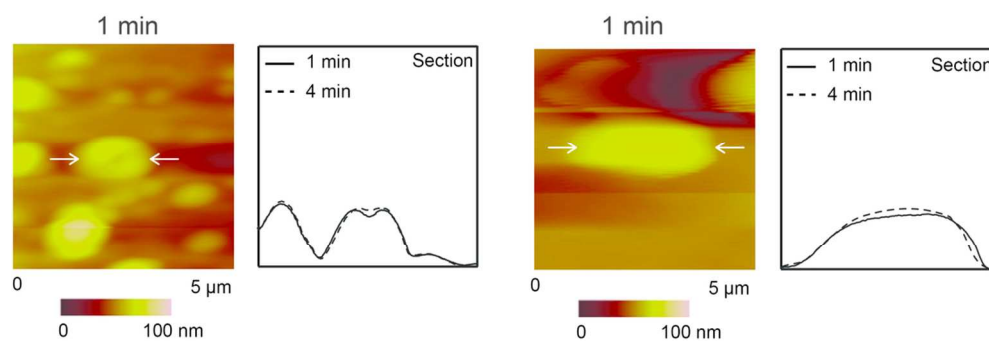
Flat punch

Examples of compression of Au 50 NP and NR at 200 μN and reverse plasticity after 4 min

Before compression

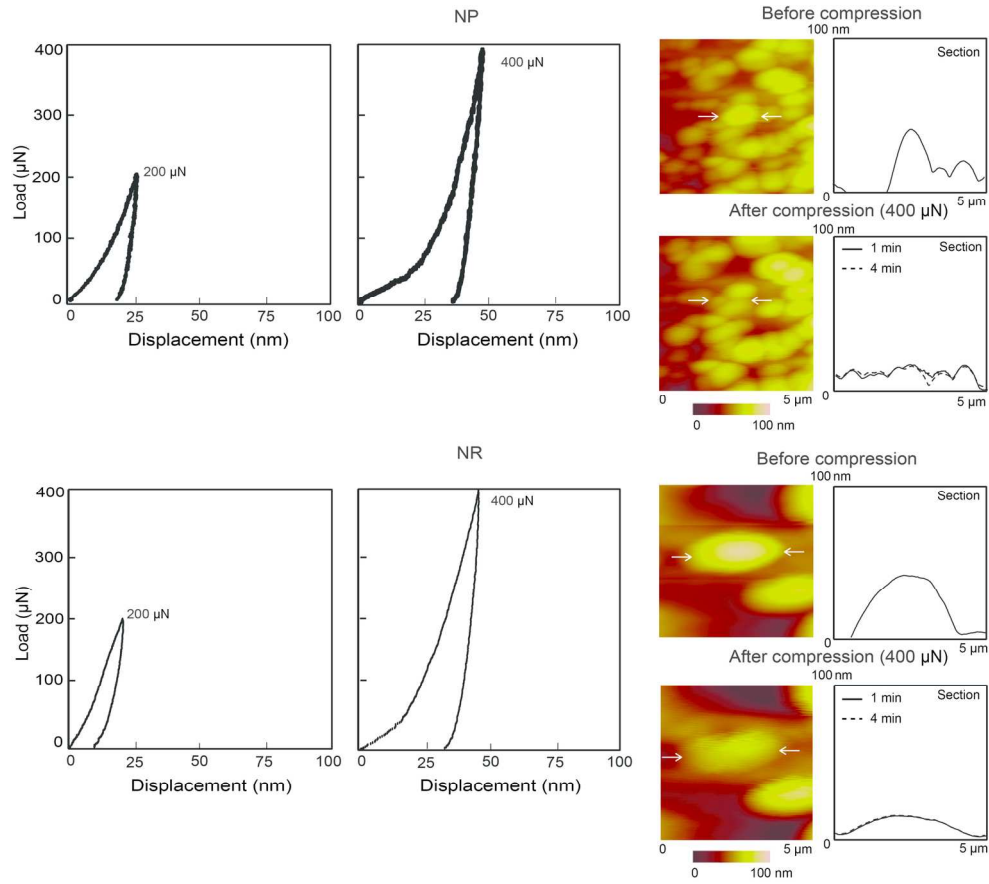


After compression



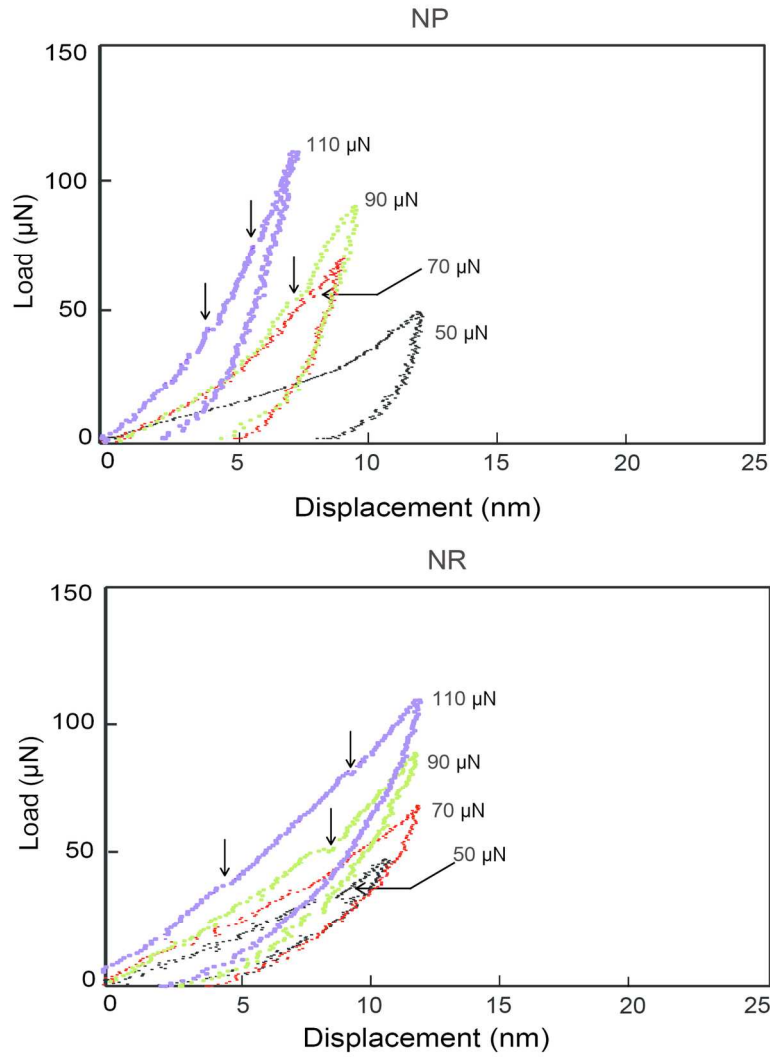
104x95mm (300 x 300 DPI)

Flat punch
Compression of Au 50 NP and NR
Examples of compression load-displacement curves
at 200 μN and 400 μN



160x155mm (300 x 300 DPI)

Flat punch
Compression of Au 50 NP and NR
Examples of repeat compression load-displacement curves
showing strain hardening and pop-in events



128x192mm (300 x 300 DPI)